Theor Chem Acc (2007) 118:295–303
DOI 10.1007/s00214-007-0249-y

REGULAR ARTICLE

A barrier-free molecular radical-molecule reaction: $^3C_2(a^3\Pi) + O_2(X^3\Sigma)$

Ming-Hui Zuo · Ji-Lai Li · Xu-Ri Huang · Hui-Ling Liu · Cai-Yun Geng · Fei Li · Chia-Chung Sun

Received: 8 September 2006 / Accepted: 21 December 2006 / Published online: 20 January 2007

Abstract The reaction of $^3C_2$ ($a^3\Pi$) radical with O_2 ($X^3\Sigma$) molecule has been studied theoretically using *ab initio* Quantum Chemistry method. Both singlet and triplet potential energy surfaces (PES) are calculated at the CCSD(T)/aug-cc-pVDZ//B3LYP/6-311+G(d) + ZPE and G3B3 levels of theory. On the singlet PES of the title reaction, it is shown that the most feasible pathway should be the O-atom of O_2 attacking the C-atom of the $^3C_2$ molecule first to form the adduct **1** CCOO, followed by the O-shift to give intermediate **2** CC(OO), and then to the major products **P1 (2CO)**. Alternatively, **1** can be directly dissociated to **P1** via transition state **TS1-P1**. The other reaction pathways are less competitive due to thermodynamical or kinetic factors. On the other hand, the pathways on the triplet PES are less competitive than those on the singlet PES in low temperature range, whereas it is not the case in high temperature ranges. On the basis of the analysis of the kinetics of all pathways through which the reactions proceed, we expect that the competitive power of reaction pathways may vary with experimental conditions for the title reaction. The reaction heats of formation calculated are in good agreement with that obtained experimentally.

Keywords Potential energy surface · Reaction mechanism · C_2 radical · Barrier-free · Radical-molecule reaction

M.-H. Zuo · J.-L. Li · X.-R. Huang (✉) · H.-L. Liu · C.-Y. Geng · F. Li · C.-C. Sun
State Key Laboratory of Theoretical and Computational Chemistry, Institute of Theoretical Chemistry, Jilin University, 130023 Changchun, People's Republic of China
e-mail: zuomh78@gmail.com

1 Introduction

Diatomic carbon molecule (C_2) is ubiquitous in the universe and found in a very wide range of sources, and is of considerable importance in combustion process [1–3], air pollution, astrophysics, and atmospheric chemistry [4,5]. In astrophysical science C_2 has been detected in widely differing environments ranging from cold regions, such as interstellar clouds [6,7], circumstellar envelopes [8], and comets [9], to hot media such as hydrocarbon flames [10], plasmas [11,12], and stellar atmospheres [13,14]. In addition, C_2 might play a crucial role in diamond growth [15]. C_2 reactions with small molecules provide particularly useful systems for detailed studies of the elementary processes in the gaseous phase [16]. The reactions of C_2 with C_2H_2, C_2H_4, N_2, NO, NO_2, H_2, H_2S and H_2O have been investigated in detail experimentally and theoretically [17–26]. Reactions with small or even zero barriers are of particular interest [27–31], especially in interstellar space where the temperature is very low (~0 K). Being one of the simplest diatomic molecules, C_2, has two low lying electronic states: the ground C_2 ($X^3\Sigma$) state and the metastable triplet state C_2($a^3\Pi$) [32], which were observed directly via LIF [32,33]. The couple states are separated by only 610 cm^{-1}. C_2 molecule exists mainly in its ground state C_2 ($X^1\Sigma$), and therefore kinetic data are required for this level. According to the published literatures, it clearly indicates that the reactivity of the triplet state has been much more studied than that of the singlet state mainly for this reason [16]. Generally, both $^1C_2$ and $^3C_2$ exist and it is difficult to assign the observations to one or the other of these states, which rapidly equilibrate in the presence of O_2 [34–36]. Arthur Fontijn's group studied the temperature dependence of the reactions

$C_2\,(X^1\,\Sigma, a^3\Pi) + O_2\,(X^3\Sigma) \rightarrow 2CO\,(X^1\Sigma, a^1\Pi)$ in a high-temperature photochemistry reactor by the 193 nm multiphoton photolysis of C_2Cl_4 [37]. The basic reaction paths suggested that, initial C_2O_2 formation followed by dissociation to produce electronically excited and ground electronic state CO molecules [34,37]. Recently, Alejandra Páramo et al. [16] reported a low-temperature gas-phase kinetics study of the reactions and collisional relaxation processes involving $C_2\,(a^3\Pi)$ and $C_2\,(X_1\Sigma)$ in collision with O_2 at temperatures from 300 to 24 K. The reactions of C_2 with O_2 are difficult to experimentally observe and characterize all possible intermediate species involved; the *ab initio* calculations method is therefore a useful tool to provide insight into such a complicated reaction system.

In this present study, we report that detailed high levels *ab initio* study of potential energy surfaces (PESs) for the title reaction, the thermodynamic properties and molecular structures of its intermediates, products, and transition states, elucidate the mechanism of the reaction. Based on the theoretical calculation, we expect that the title reaction mainly proceeds via an initial barrier-free addition process. Some of the conclusions drawn in this work may be helpful for further experimental and theoretical study of this reaction.

2 Computational methods

The calculations reported in the present investigation were carried out using the density functional theory (DFT) functional B3LYP (the hybrid three-parameter functional developed by Becke) [38–40], as implemented in the Gaussian03 program package [41]. Tran et al. have previously reported the success of the B3LYP method in predicting geometries of unsaturated chain structures, and this method produces optimized structures, at low computational cost, that compared favorably with higher level calculations [17,42]. Geometries of the reactants, products, intermediates, and transition states (TS) have been fully optimized with the B3LYP method using the 6–311+G(d) basis set. Vibrational frequencies, also calculated at the same level of theory, have been used to characterize stationary points and zero-point energy (ZPE) correction calculations. The number of imaginary frequencies for intermediates and transition states are 0 and 1, respectively. To confirm that the transition states connect between designated intermediates, intrinsic reaction coordinate (IRC) [43] calculations were performed at the B3LYP/6–311+G(d) level of theory. Zero-point vibrational energy has been calculated in the harmonic application without sealing. In order to obtain a more reliable energy, further calculations were performed with the multilevel method G3B3 [44] and the coupled-cluster CCSD(T) method with single, double, and perturbative treatment of triple excitations [45] in conjunction with the correlation-consistent polarized valence double basis sets aug-cc-pVDZ [46] were used. The B3LYP/6–311+G(d) optimized geometries were used for single-point coupled cluster calculations without reoptimization at the CCSD(T)/aug-cc-pVDZ levels. All calculations were carried out on SGI O3900 servers.

3 Results and discussion

The triplet state of C_2 has two stable isomers at B3LYP/6–311+G(d) level of theory. The bond lengths are 1.196 and 1.306 Å. The electronic structure of the 1.196 Å structure can be described as $(1\sigma_g)^2(1\sigma_u)^2(2\sigma_g)^2(2\sigma_u)(3\sigma_g)(1\pi_u)^4$. We therefore conclude that the C–C bond is a triple bond, containing a σ bond and two π bonds. The two single electrons occupied the $2\sigma_u$ and $3\sigma_g$ orbitals, respectively. Hence, its electronic state is $^3\sum_u$. On the other hand, the electronic structure of the 1.306 Åstructure is $(1\sigma_g)^2(1\sigma_u)^2(2\sigma_g)^2(2\sigma_u)^2(3\sigma_g)(1\pi_u)^3$. It contains one π bond while the two single electrons occupied the $3\sigma_g$ and π_u orbitals, respectively. Its electronic state is therefore $^3\Pi_u$. Since the $^3\Pi_u$ structure lies 27.8 kcal/mol below $^3\sum_u$, the $^3\sum_u$ state should be a triplet excited state. Therefore, we fix our attention on the reaction between $C_2\,(a^3\Pi_u)$ and $O_2\,(X^3\Sigma)$.

The optimized structural parameters of the reactants, intermediate isomers, transition states, and products for the $^3C_2(a^3\Pi) + O_2\,(X^3\Sigma)$ reaction on the singlet electronic state are shown in Fig. 1; the optimized structural parameters of the reactants, intermediate isomers, transition states, and products on the triplet electronic state are shown in Fig. 2. The total energies of all the species involved in the reaction are listed in Tables 1 and 2. Figures 3 and 4 show schematic plots of the relative energies of the singlet and triplet potential energy surfaces (PES), respectively, where the values are the CCSD(T) + ZPE and G3B3 (in parentheses) relative energies, respectively. The symbol **TSx–y** is used to denote a transition state; **x** and **y** are the corresponding isomers or products.

It should be noted that the energy of $C_2\,(X^1\Sigma, a^3\Pi) + O_2\,(X^3\Sigma)$ is set at zero as a reference for other species. As shown in Tables 1 and 2, it is clear that the results calculated at the G3B3 level are not very good, and the results calculated at the CCSD(T)/aug-cc-pVDZ// B3LYP/6–311+G(d) level are in good agreement with the experimental values [34,37,47]. So in the following discussion, we chose the results calculated at the

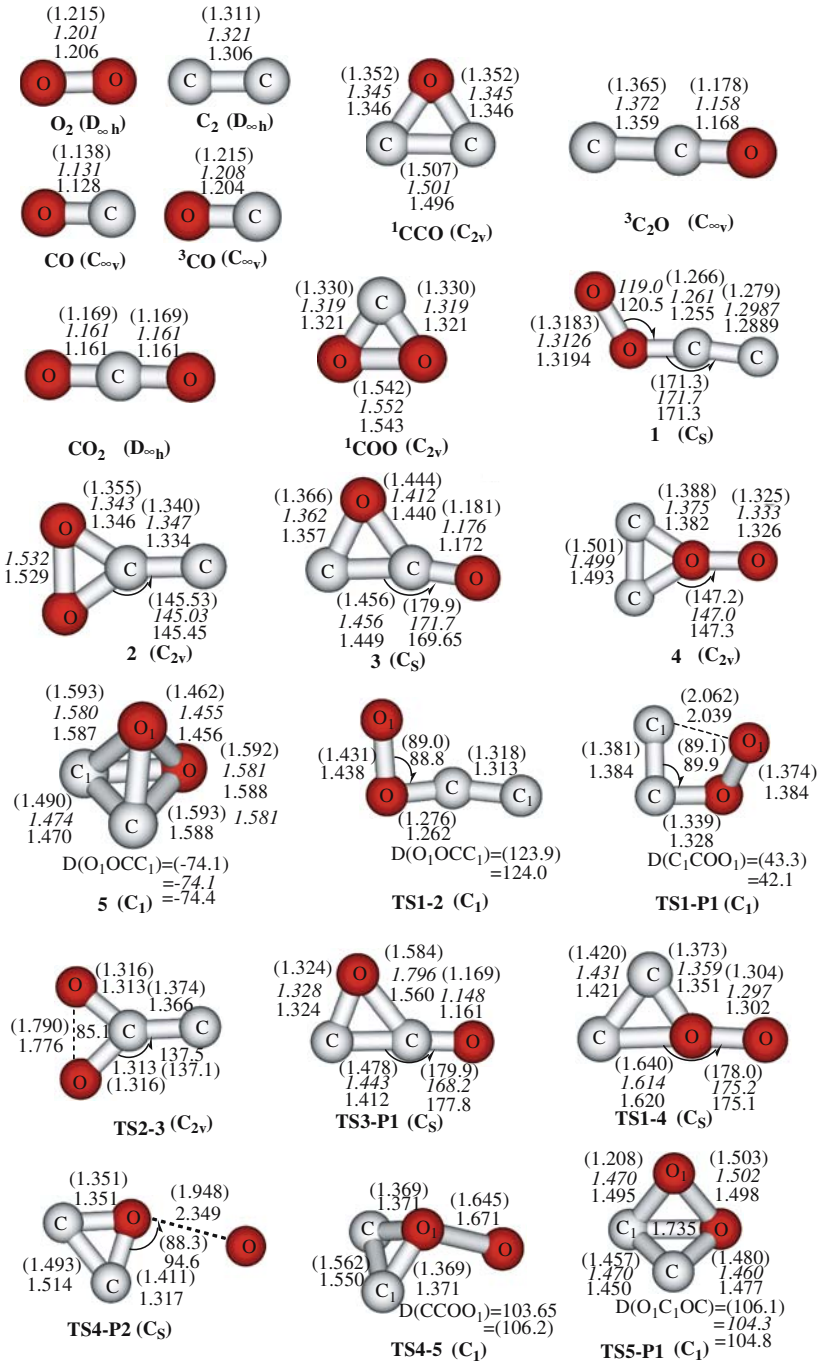

Fig. 1 Optimized geometries (Å, °) of the reactants, intermediate isomers, transition states, and products for the C_2 ($a^3\Pi$) + O_2 ($X^3\sum$) reaction. *Numbers in roman type* show the structures at the B3LYP/6–311+G(d) level of theory. *Numbers in parentheses* show the structures at the G3B3 level of theory. *Italicized numbers* denote the structures at the CCSD/6–311++G(d,p) level of theory

CCSD(T)/aug-cc-pVDZ//B3LYP/6–311+G(d) + ZPE level to analyze the change of energies along the pathways and to calculate the activation energies.

3.1 The singlet potential energy surface

There are three products, five intermediate isomers, and eight transition states present on the singlet potential energy surface. The corresponding optimized geometries and energies are shown in Fig. 1, Tables 1 and 2. As shown in Fig. 3, at the reaction entrance, only one attack mode between $^3C_2$ ($a^3\Pi$) and O_2 ($X^3\Sigma$), viz. the radical $^3C_2$ and O_2 approaches each other head to head. At the B3LYP/6–311+G(d) level, we are not able to locate any additional transition states from R to **1**. The O-atom of the molecule O_2 attacks the C-atom of the radical $^3C_2$ with no barrier in the first reaction step to form the adduct isomer **1** (CCOO). As shown in

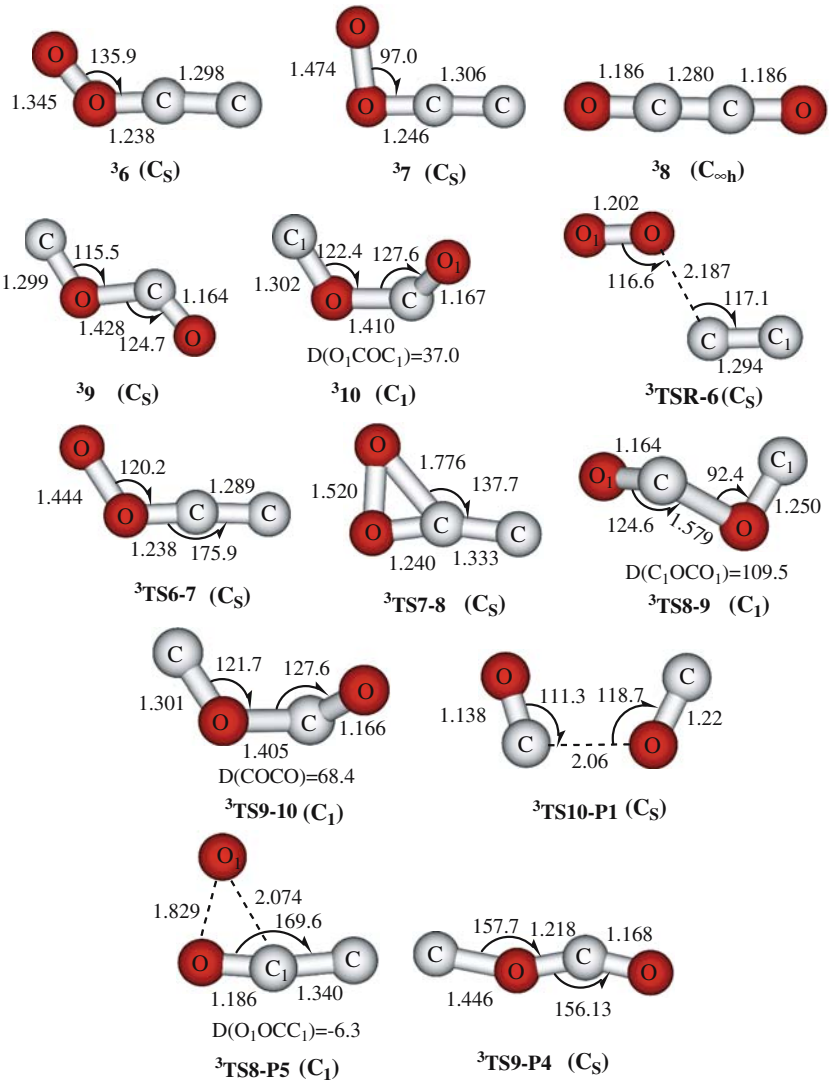

Fig. 2 Optimized geometries (Å, °) of the reactants, intermediate isomers, transition states, and products for the $^3C_2$ ($a^3\Pi$) + O_2 ($X^3\sum$) reaction. *Numbers in roman type* show the structures at the B3LYP/6–311+G(d) level of theory

Fig. 3, this is a barrierlessly exothermic step with the reaction energy of −32.57 kcal/mol at the CCSD(T)/aug-cc-pVDZ//B3LYP/6–311+G(d) + ZPE level of theory. Indeed, the dissociation curve of the C—O bond in **1** to approach the reactants is worked out via point-wise optimization method, that is, we calculated the energy by changing the atom distance point by point while the remaining geometrical parameters are fully optimized with each point. From Fig. 5, we can clearly see that the energy of the isomer OO···CC increases point by point from the equilibrium geometry **1** as the distance between the side C-atom and the O-atom increases. On account of not finding a 'hill' (character of transition state) on the curve in the region of 1.3–3.0 Å(distance-axis), we therefore expect that the O-atom may directly adduct to the C-atom of radical $^3C_2$ to form **1**.

Clearly, **1** is an energy-rich species and may make the reaction easier to go through the subsequent reaction steps. From the **1**, there are five isomerization and dissociation pathways that can be expressed as follows:

Path RP1(1): **R** → **1** → **TS1-2** → **2** → **TS2-3** → **3** → **TS3-P1** → **P1**
Path RP1(2): **R** → **1** → **TS1-P1** → **P1**
Path RP1(3): **R** → **1** → **TS1-4** → **4** → **TS4-5** → **5** → **TS5-P1** → **P1**
Path RP2: **R** → **1** → **TS1-4** → **4** → **TS4-P2** → **P2**
Path RP3: **R** → **1** → **TS1-2** → **2** → **P3**

Obviously, all of the five isomerization-dissociation pathways possess the same initial steps of the reaction, i.e., **R** → **1**. First, from the isomer **1** CCOO with the energy of −32.57 kcal/mol, the pathway RP1(1) can reach the products **P1**(2CO) easily by going through **TS1-2**, isomer **2** (OO)CC, **TS2-3**, isomer **3** (CO)CO, and **TS3-P1** in succession with the energies of −6.94, −47.5,

Table 1 Theoretical predication of the total energy (hartrees), harmonic ZPE (hartrees), and relative energies (kcal/mol) for products of $^3C_2$ ($a^3\Pi$) + O_2 ($X^3\sum$) reaction at different levels of theory

Species	B3LYP/ 6–311+G(d)	ZPE	CCSD(T)/ aug-cc-pVDZ	G3B3	ΔE^1	ΔE^2	Exp
R($^3C_2$ + $^3O_2$)	−226.3085278	0.007568	−225.7535006	−226.1372149	0.0	0.0	
P1(CO + CO)	−226.6880186	0.010082	−226.1464364	−226.5399386	−244.99 −250.60[d] −250.59[e]	−252.71	−250.25[a]
P2(^{3}O + ^{3} CCO)	−226.3245520	0.007514	−225.7795570	−226.1607676	−16.38 −14.56[d] −14.40[e]	−14.78	−17.69[b]
P3(^{3}C + ^{1} COO)	−225.9000166	0.006662	−225.7281100	−226.1086861	15.36 14.70[d] 16.25[e]	17.90	
P4(^{3}C + CO_2)	−226.5041817	0.010164	−225.9498390	−226.3342020	−121.58 123.21[d] 121.74[e]	−123.61	−120.12[a]
P5(^{3}O + ^{3} C_2O)	−226.3949892	0.008002	−225.8359089	−226.2171068	−51.44 −50.75[d] −50.54[e]	−50.13	−48.4 ± 4.61[c]
P*(CO + ^{3} CO)	−226.4832362	0.009103	−225.9288830	−226.3209542	−109.09 −111.59[d] −111.53[e]	−115.30	

ΔE^1 represents the relative energies calculated at the CCSD(T)/aug-cc-pVDZ//B3LYP/6–311+G(d)+ZPE level of theory
ΔE^2 represents the relative energies calculated at the G3B3 level of theory
[a] Experimental Reaction Heats are given in kcal/mol (see Ref. [34])
[b] Experimental Reaction Heats are given in kcal/mol (see Ref. [37])
[c] Experimental Reaction Heats are given in kcal/mol (see Ref. [47])
[d] Represents the relative energies calculated at the CCSD(T)/cc-pVTZ//B3LYP/cc-pVTZ + ZPE level of theory
[e] Represents the relative energies calculated at the CCSD(T)/cc-pVTZ//CCSD/cc-pVTZ + ZPE level of theory

−43.8, −153.4, and −154.3 kcal/mol, respectively. It is a successive O-shifts mechanism, i.e., the side O-atom shifts to the inner C-atom and then to the side C-atom. Since all the energies of the transition states and isomers in the pathway RP1(1) are lower than that of the reactants, the rate of this pathway should be very fast. It should be noted that the relative energy of **TS3-P1** is lower than that of **3**, which the stationary point **TS3-P1** is connected with through IRC calculation. The problem about the upside-down energies of **TS3-P1** and **3** lies in the theoretical computational method we adopted during the calculation. As introduced in Sect. 2 all energies presented in the paper are at the CCSD(T)/aug-cc-pVDZ//B3LYP/6–311+G(d) + ZPE level or G3B3. If the potential energy barrier is very low and the ZPE correction is significant, this treatment of the energies can lead to a barrier less than zero. Because it has been suggested that DFT calculations can underestimate barriers' height by kilocalories per mole, such a situation should not be over-interpreted, but can be taken as an indication of the lack of a significant barrier [48]. On the other hand, isomer **2** CC(OO) can transform to products **P3** (**^{3}C + ^{1} COO**) directly in pathway RP3. The dissociation curve of the C–C bond in isomer **2** CC(OO) to approach the products **P3** (**^{3}C + ^{1} COO**) is worked out at the B3LYP/6–311+G(d) level of theory via point-wise optimization method in Fig. 5. With a large quantity of heat required in the endergonic dissociation process, the C-atom formation mechanism may rule out its significance in atmospheric chemistry at lower temperature, and even at higher temperatures. Second, for pathway RP1(2), isomer **1** can overcome a 31.57 kcal/mol energy barrier (**TS1-P1**), directly to educts **P1**. This is a four-center ring formation–decomposition mechanism. Because the rate-determining energy barrier (31.57) of Path RP1(2) is higher than the ones of Path RP1(1) (25.67), pathway Path RP1(2) should be less competitive than pathway Path RP1(1). Furthermore, for pathway Path RP1(3), isomer 1 can also transform to P1 through a successive C-shift and O-rock and four-center cage decomposition process. Because it possess two high lying transition states, **TS1-4** (14.3) and **TS4-5** (37.1), we can safely draw the conclusion that pathway Path RP1(3) is less competitive than pathway Path RP1(1) in lower temperature range. Although, the temperature is considerably high, the reactants may overcome

Table 2 Theoretical predication of the total energy (hartrees), harmonic ZPE (hartrees), and relative energies (kcal/mol) for products, intermediate isomers and transition states of the $^3C_2$ ($a^3\Pi$) + O_2 ($X^3\sum$) reaction at different levels of theory

Species	B3LYP/ 6–311+G(d)	ZPE	CCSD(T)/ aug-cc-pVDZ	G3B3	ΔE^1	ΔE^2
1	−226.3553198	0.011560	−225.8093938	−226.2033133	−32.57	−41.48
2	−226.3793868	0.011782	−225.8334386	−226.2288960	−47.52	−57.53
3	−226.5525468	0.012999	−226.0033513	−226.4005080	−153.38	−165.22
4	−226.2866384	0.010325	−225.7353301	−226.1303259	13.13	4.32
5	−226.3227929	0.010211	−225.7892368	−226.1814862	−20.77	−27.78
^{3}6	−226.3580524	0.010432	−225.7771989	−226.1749042	−13.07	−23.65
^{3}7	−226.3604959	0.010003	−225.7828376	−226.1757337	−16.88	−24.17
^{3}8	−226.6364617	0.013693	−226.0480001	−226.4494089	−180.96	−195.90
^{3}9	−226.5028475	0.011641	−225.9393704	−226.3291413	−114.08	−120.44
^{3}10	−226.4973442	0.011358	−225.9326546	−226.3231019	−110.04	−116.65
TS1-4	−226.2808060	0.009375	−225.7324600	−226.1254970	14.34	7.35
TS1-2	−226.3163972	0.009462	−225.7664507	−226.1602939	−6.94	−14.48
TS1-P1	−226.2948115	0.009889	−225.7573550	−226.1441381	−0.96	−4.34
TS2-3	−226.3671753	0.009605	−225.8252613	−226.2189586	−43.75	−51.29
TS3-P1	−226.5530392	0.011965	−226.0038280	−226.4009398	−154.32	−165.49
TS4-5	−226.2350563	0.007925	−225.6947033	−226.0815636	37.12	34.92
TS4-P2	−226.2298571	0.007276	−225.6911152	−226.0748670	38.96	39.12
TS5-P1	−226.3133084	0.008566	−225.7760669	−226.1676709	−13.53	−19.11
^{3}TSR-6	−226.3038490	0.008318	−225.7479119	−226.1485329	3.98	−7.10
^{3}TS6-7	−226.3550310	0.008810	−225.7803398	−226.1740305	−16.06	−23.10
^{3}TS7-8	−226.3571554	0.009147	−225.7892144	−226.1806861	−21.42	−27.28
^{3}TS8-9	−226.4996734	0.010617	−225.9339188	−226.3250459	−111.30	−117.87
^{3}TS9-10	−226.4972216	0.010948	−225.9322986	−226.3236591	−110.08	−117.00
^{3}TS10 − P*	−226.4738866	0.009555	−225.9101567	−226.3027777	−97.06	−103.89
^{3}TS8-P5	−226.3494209	0.009062	−225.7953472	−226.1918354	−25.32	−34.27
^{3}TS9-P4	−226.4767129	0.009247	−225.8997650	−226.2958202	−90.73	−99.53

$\Delta\mathbf{E^1}$ represents the relative energies calculated at the CCSD(T)/aug-cc-pVDZ//B3LYP/6–311+G(d)+ZPE level of theory. $\Delta\mathbf{E^2}$ represents the relative energies calculated at the G3B3 level of theory

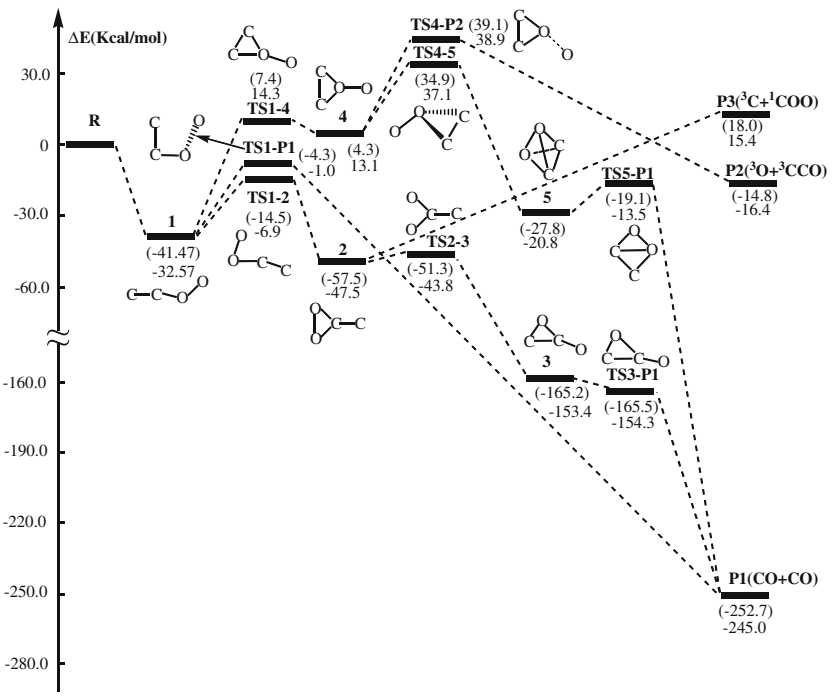

Fig. 3 Singlet potential energy surface (PES) for the $^3C_2$ ($a^3\Pi$) + O_2 ($X^3\Sigma$) reaction at the CCSD(T)/aug-cc-pVDZ//B3LYP/6–311+G(d) + ZPE and G3B3 (*in parentheses*) levels of theory

the barrier of **TS4-5** and give to educts **P1**. In pathway RP2, isomer **4** OO(CC) can surmount transition state **TS4-P2** (38.9), leading to product **P2** (**^{3}O+^{3}CCO**). Considering possessing of the highest transition state on the singlet PES, we expect that Path RP2 can be safely ruled out.

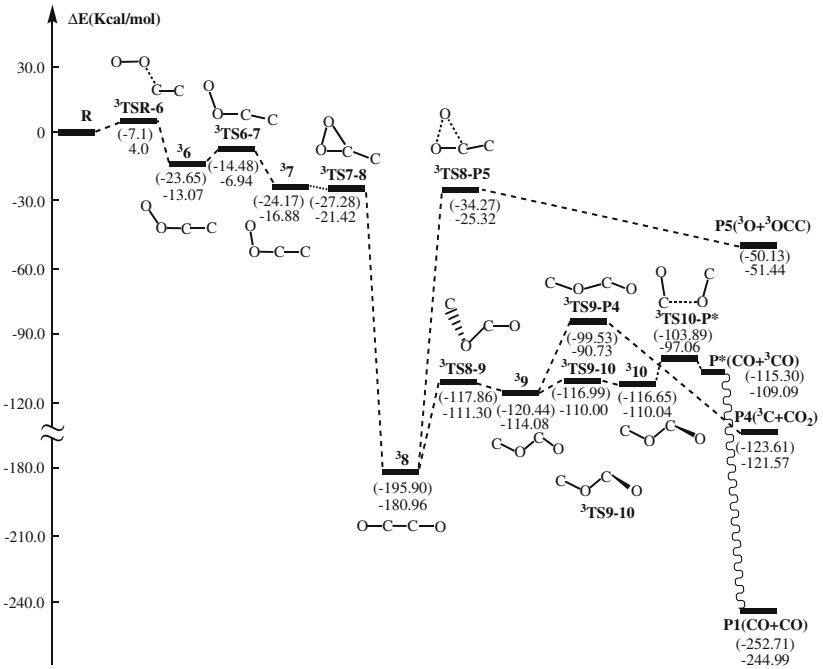

Fig. 4 Triplet potential energy surface (PES) for the $^3C_2$ ($a^3\Pi$) + O_2 ($X^3\Sigma$) reaction at the CCSD(T)/aug-cc-pVDZ//B3LYP/6–311+G(d) + ZPE and G3B3 (*in parentheses*) levels of theory

To briefly summarize, pathway Path RP1(1) and Path RP1(2) are major pathways among all pathways mentioned earlier. The pathway Path RP1(1) should be more competitive than RP1(2) at all temperature ranges. Consequently, carbon monoxide (CO) is the major product of the title reaction.

Before ending, we should mention that, for structures the **1**, **2**, **3**, **4**, **5**, **TS1-4**, **TS3-P1**, **TS5-P1** and all products, we have carried out the cost-expensive geometrical calculations at the CCSD/6–311++G(d,p) level of theory to test the reliability of the present DFT-based calculations. Fortunately, we find that the obtained bond lengths and bond angles are generally in good agreement with the B3LYP/6–311+G(d) values, as shown in Fig. 1. This indicates that the B3LYP/6–311+G(d) method can be safely used for the study of the C_2 ($a^3\Pi$) + O_2 ($X^3\Sigma$) system.

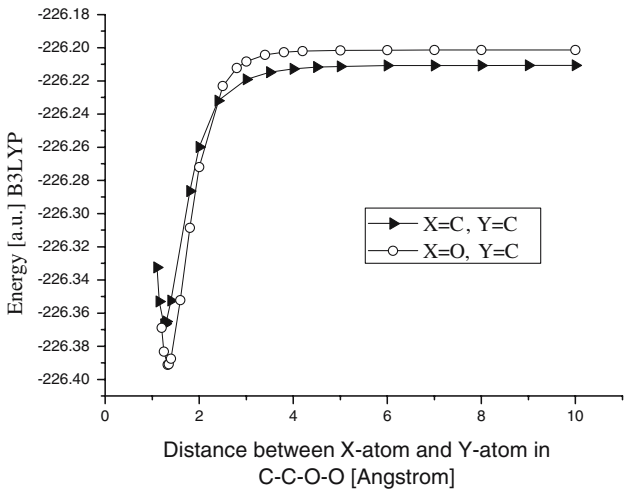

Fig. 5 Bond dissociation curves calculated via point-wise optimized method at the B3LYP/6–311+G(d) level of theory

3.2 The triplet potential energy surface

There are three pathways that can be seen on the triplet potential energy surface:

Path RP1(4): **R** → ^{3}**6** → ^{3}**7** → ^{3}**8** → ^{3}**9** → ^{3}**10** → **P***(**CO** + ^{3}**CO**) → **P1**(**2CO**)
Path RP5: **R** → ^{3}**6** → ^{3}**7** → ^{3}**8** → **P5**(^{3}**O** + ^{3}**OCC**)
Path RP4: **R** → ^{3}**6** → ^{3}**7** → ^{3}**8** → ^{3}**9** → **P4**(^{3}**C** + **CO$_2$**)

these three pathways possess the same initial steps of the reaction, i.e., **R** → ^{3}**6** → ^{3}**7** → ^{3}**8**. It is an O-adduct-shift mechanism. The difference of the three pathways is in how ^{3}**8** OCCO(−180.96) changes to **P1**, **P4**, and **P5**. For pathway RP1(4), ^{3}**8** transforms to **P1 (2CO)** by going successively through ^{3}**TS8-9**(−111.30), ^{3}**9**(−114.08), ^{3}**TS9-10**(−110.0), ^{3}**10**(−110.04), ^{3}**TS10-P*** (−97.05), and **P*** (−109.09). We should mention here that the bond lengths of the two **CO** molecules in complex **P*** are different according to our IRC calculation at the B3LYP/6–311+G(d) level of theory as shown in Fig. 6. In fact, one of them is a triplet ^{3}**CO** and the other is a singlet ^{1}**CO**. It is creditable that the **P***on the triplet

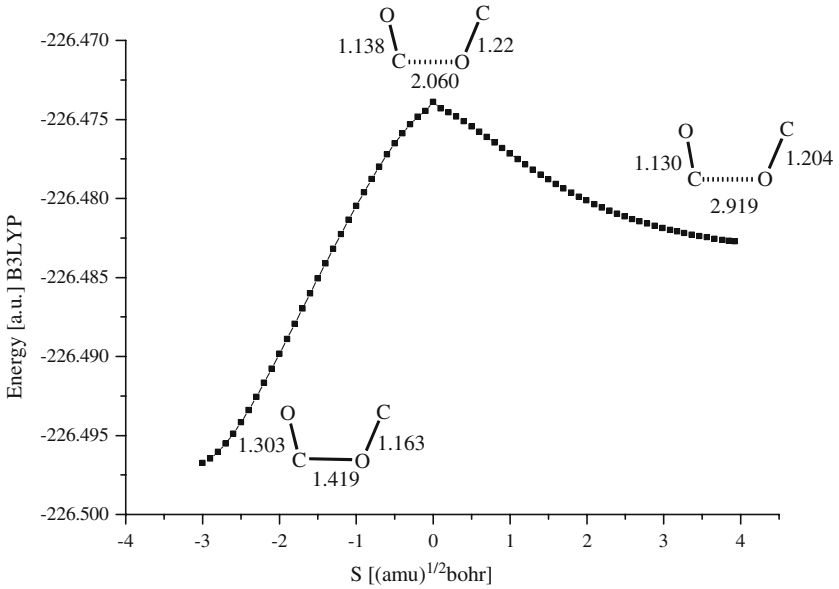

Fig. 6 Bond dissociation curve calculated via IRC calculations at the B3LYP/6–311+G(d) level of theory

surface can transform to the **P1** on the singlet surface. Detlef Schröder et al. have located a minimum energy crossing point (MECP) between the singlet and triplet surfaces of $\mathbf{C_2O_2}$ [49]. In their opinion, the neutral OCCO is intrinsically short-lived in its singlet state, and it will dissociate spontaneously and spin-allowed into two singlet ^{1}**CO** molecules. While the dissociation process from triplet **OCCO** to a singlet ^{1}**CO** and a triplet ^{3}**CO** has to absorb a great deal of energy. However, since the MECP has been located, the efficient triplet **OCCO** dissociation pathway is a curve crossing channel through the MECP to the singlet surface, and the production is two singlet ^{1}CO molecules. The work of Detlef Schröder et al. gives us a very strong evidence to believe that our product **P*** can transform to **P1** through the MECP.

On the other hand, from ^{3} **8** OCCO (−180.96), pathway RP5 can reach the products **P5**(^{3}**O** + ^{3} **OCC**) by overcoming the transition state ^{3}**TS8** − **P5** (−25.32), a very high energy barrier. Furthermore, pathway RP4 possesses the same reaction step **38** $\rightarrow^3$ **9** as pathway RP1(4). However, ^{3}**9** can directly eliminate ^{3}C via ^{3}**TS9** − **P4** (−90.73) in pathway RP4. Since the barriers involved in all of the three pathways are moderate ($\Delta E < 4$ kcal/mol) and the formation of the final products are exoergic ($\Delta E > -50$ kcal/mol), both kinetic and thermodynamic considerations support the viability of such channels.

3.3 Comparison with experiments

Recently, both Páramo et al. [16] and Fontijn' et al. [37] studied the gas-phase kinetics of the title reaction, the former in the temperature range from 24 to 300 K and the latter at high temperature ranges. They fixed their attention on the observation of products **P1**, although A. Fontijn suggested in addition to two rovibrationally excited CO molecules, the possible direct "further products" are C_2O_2, $C_2O + O$, and $CO_2 + C$, which could be in excited states [37]. However, they did not give any information about the reaction mechanism and potential products. According to our results, it is shown that the most feasible pathway is on the singlet PES of the title reaction, and the most feasible pathway should be the O-atom of O_2 attacking the C-atom of the $^3C_2$ molecule first to form the adduct **1** CCOO in a deep potential well, followed by an O-shift to give **2** CC(OO), and then dissociation to the major products **P1 (2CO)**. Since there is no barrier for this pathway, the title reaction is expected to be very fast. This is qualitatively consistent with the experimental result [34,37,47]. On the other hand, it should be pointed out that our theoretical results indicate that the title reaction occurring on the triplet PES may be competitive with that on the singlet PES at high temperature. This situation differs from that of our earlier investigation on the reaction between $^3C_2$ and NO [17]. As shown in Figs. 3 and 4, we expect that products **P1** may be produced through the singlet PES, while products **P4** and **P5** are produced on the triplet PES. Further theoretical and experimental studies are desirable.

4 Conclusions

The mechanism of the $^3C_2(a^3\Pi) + O_2(X^3\Sigma)$ reaction is elucidated by means of ab initio calculations at the

CCSD//B3LYP, G3B3, and CCSD(T) levels of theory. The major pathway is Path RP1(1): **R** → **1** → **2** → **3** → **P1**(**2CO**) on the singlet potential energy surface. And **R** $\rightarrow^3$ **6** $\rightarrow^3$ **7** $\rightarrow^3$ **8** $\rightarrow^3$ **9** $\rightarrow^3$ **10** → **P***(**CO** $+^3$ **CO**) → **P1**(**2CO**) on the triplet potential energy surface with **P1** expected to be the main product. The singlet pathway is barrierless. Other pathways on the singlet and triplet PESs may be less competitive for both kinetic and thermodynamic reasons. Further theoretical and experimental studies are desirable to provide some useful insight into the mechanism of the C_2 radical reaction. Compared with their action between the well-known NO and $^3C_2(a^3\Pi)$ radical, the barrier-free $O_2\,(X^3\Sigma)$ reaction with $^3C_2\,(a^3\Pi)$ is expected to be of unique importance.

Acknowledgments This work is supported by the National Natural Science Foundation of China (nos. 20073014 and 20103003), Excellent Young Teacher Foundation of the Ministry of Education of China, Excellent Young Foundation of Jilin Province and Technology Development Project of Jilin Province (no. 20050906-6). The authors are thankful for the reviewers' invaluable comments.

References

1. Gaydon AG, Wolfhard HG (1979) Flames, their structure, radiation, and temperature. Chapman & Hall, New York
2. O'Brien SC, Heath JR, Curl RF, Smalley RE (1988) J Chem Phys 88:220
3. Perry MD, Raff LM (1994) J Phys Chem 98:4375
4. Weltner JW, Van Zee R (1989) Chem Rev 89:1713
5. Kaiser RI (2002) Chem Rev 102:1309
6. Cecchi-Pestellini C, Dalgarno A (2002) Mon Not R Astron Soc 331:L31
7. Oka T, Thorburn JA, McCall BJ, Friedman SD, Hobbs LM, Sonnentrucker P, Welty DE, York DG (2003) Astrophys J 582:823
8. Bakker EJ, van-Dishoeck EF, Waters LBFM, Schoenmaker T (1997) Astron Astrophys 323:469
9. A'Hearn MF, Millis RC, Schleicher DO, Osip DJ, Birch PV (1995) Icarus 118:223
10. Baronavski AP, McDonald JR (1997) J Chem Phys 66:3300
11. Rennick CJ, Smith JA, Ashfold MNR, Orr-Ewing A (2004) J Chem Phys Lett 383:518
12. Gordillo-Vazquez FJ, Albella JM (2003) J Appl Phys 94:6085
13. McKellar A, Astron JR (1960) Soc Can 54:97
14. Brault JW, Delbouille L, Grevesse N, Roland G, Sauval AJ, Testerman L (1982) Astron Astrophys 108:201
15. Rabeau JR, John P, Wilson JIB (2004) J Appl Phys 96:6724
16. Páramo A, Canosa A, Le Picard SD, Sims IR (2006) J Phys Chem A 110:3121
17. Wei ZG, Huang XR, Zhang SW, Sun YB, Qian HJ, Sun CC (2004) J Phys Chem A 108:6771
18. Wei ZG, Huang XR, Sun YB, Liu JY, Sun CC (2004) J Mol Struct (Theochem) 671:133
19. Wang JH, Han KL, He GZ, Li ZJ (2003) Chem Phys Lett 368:139
20. Balucani N, Mebel MA, Lee YT, Kaiser RI (2001) J Phys Chem A 105:9813
21. Kaiser RI, Le TN, Nguyen TL, Mebel AM, Balucani N, Lee YT, Stahi F (2002) Faraday Discuss 119:51
22. Ding YH, Li ZS, Huang XR, Sun CC (2000) J Chem Phys 113:1745
23. Zhang X, Ding YH, Li ZS, Huang XR, Sun CC (2000) Chem Phys Lett 330:577
24. Kruse T, Roth P (1997) J Chem Phys Lett 101:2138
25. Kaiser RI, Yamada M, Osamura Y (2002) J Phys Chem 106:4825
26. Wang JH, Han KL, He GZ, Li ZJ, Morris VR (2003) J Phys Chem A 107:9825
27. Wang ZX, Huang MB, Liu RZ (1997) Can J Chem 75:996
28. Butler JE, Fleming JW, Lin MC (1981) Chem Phys 35:355
29. Berman MR, Lin MC (1983) Chem Phys 82:435
30. Faure A, Rist C, Valiron P (1999) Chem Phys 241:29
31. Carl SA, Elsamra RMI, Kulkarni RM, Nguyen HMT Peeters J (2004) J Phys Chem A 108:3695
32. Herzberg G (1950) Spectra of diatomic molecules. Van Nostrand, Princeton
33. Huang CS, Zhao DF, Pei LS, Chen CX Chen Y (2004) Chem Phys Lett 389:230
34. Reisler H, Mangir M, Wittig C (1980) Chem Phys 47:49
35. Mangir MS, Reisler H, Wittig C (1980) J Chem Phys 73:829
36. Filseth SV, Hancock G, Meier K (1979) Chem Phys Lett 61:288
37. Fontijn A, Fernandez A, Ristanovic A, Randall MY, Jankowiak JT (2001) J Phys Chem A 105:3182
38. Becke AD (1988) Phys Rev A 38:3098
39. Becke AD (1993) J Chem Phys 98:1372
40. Becke AD (1993) J Chem Phys 98:5648
41. Frisch MJ, Trucks GW, Schlegel HB, Scuseria GE, Robb MA, Cheeseman JR, Montgomery JA Jr, Vreven T, Kudin KN, Burant JC, Millam JM, Iyengar SS, Tomasi J, Barone V, Mennucci B, Cossi M, Scalmani G, Rega N, Petersson GA, Nakatsuji H, Hada M, Ehara M, Toyota K, Fukuda R, Hasegawa J, Ishida M, Nakajima T, Honda Y, Kitao O, Nakai H, Klene M, Li X, Knox JE, Hratchian HP, Cross JB, Adamo C, Jaramillo J, Gomperts R, Stratmann RE, Yazyev O, Austin AJ, Cammi R, Pomelli C, Ochterski JW, Ayala PY, Morokuma K, Voth GA, Salvador P, Dannenberg JJ, Zakrzewski VG, Dapprich S, Daniels AD, Strain MC, Farkas O, Malick DK, Rabuck AD, Raghavachari K, Foresman JB, Ortiz JV, Cui Q, Baboul AG, Clifford S, Cioslowski J, Stefanov BB, Liu G, Liashenko A, Piskorz P, Komaromi I, Martin RL, Fox DJ, Keith T, Al-Laham MA, Peng CY, Nanayakkara A, Challacombe M, Gill PMW, Johnson B, Chen W, Wong MW, Gonzalez C, Pople JA (2003) Revision B.03, Gaussian, Inc., Pittsburgh
42. Tran KM, McAnoy AM, Bowie JH (2004) Org Biomol Chem 2:999
43. Gonzalez C, Schlegel HB (1990) J Phys Chem 94:5523
44. Baboul AG, Curtiss LA, Redfern PC (1999) J Chem Phys 110:7650
45. Purvis GD, Bartlett RJ (1982) J Chem Phys 76:1910
46. Woon DE, Dunning TH Jr (1993) J Chem Phys 98:1358
47. Shackleford WL, Mastrup FN, Kreye WC (1972) J Chem Phys 57:3933
48. Li JL, Huang XR, Bai HT, Geng CY, Yu GT, Sun CC (2005) J Mol Struct (Theochem) 730:205
49. Schröder D, Heinemann C, Schwarz H, Harvey JN, Dua S, Blanksby SJ, Bowie JH (1998) Chem Eur J 4:2050